Atomic and electronic structure of the NiAl(111) surface

M. H. Kang,* S.-C. Lui,† E. J. Mele, and E. W. Plummer
The Laboratory for Research on the Structure of Matter, University of Pennsylvania, Philadelphia, Pennsylvania 19104-6202

D. M. Zehner
Solid State Division, Oak Ridge National Laboratory, Oak Ridge, Tennessee 37831
(Received 25 August 1989)

There are two possible terminations for the ideal NiAl(111) surface, i.e., all Al or all Ni on the surface atomic layer. We investigate which termination occurs on the NiAl(111) surface by comparing the pseudopotential electronic band structure of a Ni-terminated and an Al-terminated NiAl(111) surface with the angle-resolved photoemission data on a NiAl(111) sample. The measured surface band structure shares common features partly with that of the Ni termination and also partly with that of the Al termination, which supports the theory that the real NiAl(111) surface is composed of both Ni- and Al-terminated (111) domains, as suggested by a recent low-energy electron diffraction (LEED) study. We also determine the relaxation of the two outermost atomic layers for both terminations by the pseudopotential total-energy calculations and compare them with the LEED results. We find that the present results are in good agreement with the LEED analysis for Ni termination, but in qualitative disagreement for Al termination.

I. INTRODUCTION

NiAl is an ordered alloy with the CsCl structure. Ni is a $3d$ transition element characterized by the strongly localized valence d electrons and Al is an sp-electron element. The nature of the interatomic bonding in NiAl is very different from pure Ni and pure Al. Due to the inhomogeneous atomic composition, NiAl surfaces have many interesting properties not present in the monatomic crystal surfaces. Recently, as a prototype of multicomponent surfaces, the NiAl(110) surface has been investigated extensively by several experimental and theoretical tools.[1-5] The atomic structure, the electronic structure, and the vibrational properties of this surface are now well understood. Our knowledge on the NiAl(111) surface is very limited, because the surface structure (composition) is still in question.

The NiAl(111) surface is quite different in its atomic structure from the previously well-studied NiAl(110) surface. It is useful to compare briefly the characteristics of the two atomic structures. NiAl(110) is an ordered two-component surface where each atomic layer parallel to the surface contains both Ni and Al atoms in a rectangular lattice with the stoichiometric composition of the bulk, and its large interlayer spacing ($d_0=2.04$ Å) allows rapid healing of the electron density to its bulk form in the subsurface region. As a result, this system tends to keep the second atomic layer stable in a bulk configuration. This made the one-layer relaxation model practical in theoretical approach[4,5] and the results were very successful in giving a theoretical interpretation of the measured structure-related properties of NiAl(110).

On the other hand, in NiAl(111) each atomic layer parallel to the surface forms a triangular lattice with only one species of atoms (Ni or Al), i.e., a Ni layer and an Al layer are alternating along the [111] direction (Fig. 1). Therefore, the ideal NiAl(111) surface can have two possible terminations: Ni termination [i.e., Ni/NiAl(111)] or Al termination [i.e., Al/NiAl(111)]. In addition, NiAl(111) has a very open structure with a short interlayer spacing ($d_0=0.83$ Å) and a low atomic density in the surface plane, and so the deeper layers should be included in the consideration of surface properties. These many structural degrees of freedom have delayed an adequate theoretical approach to the atomic structure of NiAl(111). Although there are several experimental data on the termination of NiAl(111), their analysis leads to somewhat contradicting conclusions as follows.

Noonan and Davis[6] investigated the atomic structure of this surface through a low-energy electron diffraction (LEED) analysis. They carried out dynamical LEED I-V calculations for both Ni/NiAl(111) and Al/NiAl(111) using a two-layer relaxation model and compared them with measured LEED I-V spectra. Surprisingly they found that the best agreement between measured and calculated I-V spectra is obtained by neither a Ni/NiAl(111) nor an Al/NiAl(111), but by assuming that the surface is a 50%-50% mixture of two ordered domains, Ni/NiAl(111) and Al/NiAl(111). They suggested a structural model of NiAl(111) where the surface is composed of large terraces and steps with a single interplanar spacing between adjacent terraces.[7] They also determined the relaxation of the two outermost atomic layers in each domain. Franchy *et al.*[8] carried out electron energy-loss spectroscopy (EELS) experiments to study the adsorption properties of S, CO, and O on NiAl(111) and used the results to obtain information on the termination of NiAl(111). From the comparison of the data with those obtained for the pure Ni(111) surface and Al(111) surface, they found that the adsorption of S and CO can be explained well by Ni/NiAl(111) and that Al/NiAl(111) is unlikely in many respects. These EELS

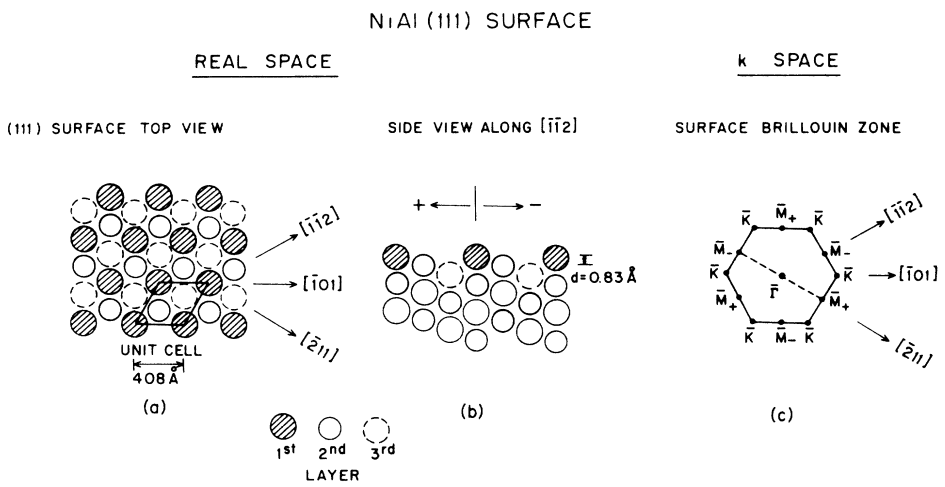

FIG. 1. Real- and reciprocal-space representation of the NiAl(111) surface: (a) Top view of an ideal NiAl(111) surface, (b) side view along the $[\bar{1}\bar{1}2]$ direction, (c) surface Brillouin zone showing the two inequivalent $\bar{M}$ points.

results indicate that the NiAl(111) surface is probably Ni terminated, but can not exclude the possibility of a mixed phase system with domains of either termination. Wendelken[9] measured the average step height of a vicinal NiAl(111) surface with a high step density using energy-dependent LEED beam-shape analysis. With an equal probability for either termination, suggested by Noonan and Davis,[6] we can expect an average step height of a single atomic layer. However, Wendelken's results showed that the average height is two interlayer spacings, which suggests that one specific termination is preferred.

It is difficult to draw a unified picture of the atomic structure of NiAl(111) from the above experimental results because they are incompatible with each other. Different approaches to this surface are desirable. In the present study we apply the pseudopotential density-functional formalism and the angle-resolved ultraviolet photoelectron spectroscopy (ARUPS) for the atomic and the electronic structure of this surface. The pseudopotential total-energy-calculation scheme was successful in determining the rippled atomic structure of NiAl(110).[4] However, a direct comparison of the total energies of the individual terminations is not possible in the NiAl(111) surface since the stoichiometry of the thin films used to model each termination is inequivalent. Hence, we approach to this problem in the following way. First, we calculate the relaxation of NiAl(111) for both terminations and compare them with the previous LEED analysis.[6] We will treat the two terminations separately on an equal footing and determine the relaxation pattern of the individual terminations. Although this study doesn't give an answer to the question on the termination, it will serve as an indirect test of the validity of the structural model given by LEED analysis (Sec. II). Second, we can utilize the electronic structure of NiAl(111) to extract information about the surface termination. The electronic band structure is sensitive to the underlying atomic structure. We measure the surface band structure of a real NiAl(111) sample using ARUPS and calculate the band structure of Ni/NiAl(111) and Al/NiAl(111) in their relaxed atomic structures. The comparison of the measured and the calculated electronic structures can yield a clue on the termination (Sec. III).

II. RELAXATION OF THE Ni- AND Al-TERMINATED NiAl(111) SURFACE

In the present calculation, the NiAl(111) surface is simulated by a periodic slab geometry. We choose a slab thickness of nine atomic layers for Ni/NiAl(111) and, for Al/NiAl(111), we introduce an additional Al layer on each side of the previous nine-layer slab of Ni/NiAl(111). In this way, we can clearly identify the changes in the electronic structure affected by the additional Al layer. The slabs are separated by a vacuum region of 10 interlayer spacings ($=8.33$ Å) in both terminations. We calculate the band structure and total energy of the system using the Hohenberg-Kohn-Sham local-density approximation[10,11] and the Ceperley-Alder potential for exchange and correlation as parametrized by Perdew and Zunger[12,13] and the modified mixed-basis pseudopotential formalism.[14] It has been shown through the previous studies that the modified mixed-basis scheme, which is characterized by the use of *nonoverlapping* localized basis functions, is effective in dealing with systems containing $3d$ transition elements.[4,14,15] We employ 25 optimized d orbitals and around 800 (950) plane waves for a Ni (Al) termination in the present mixed-basis set ($E_{\text{cutoff}}=10$ Ry) and choose 6 **k** points in an irreducible Brillouin zone for the charge-density calculations. We iterate the self-consistent loop until the difference in every G-space component between input and output potential is less than 0.005 Ry. At the self-consistent stage, the total-energy difference between the successive iterations is less than 0.5 mRy.

A deeper multilayer relaxation is expected in NiAl(111) because of the open nature of the system, but we wish to consider only the relaxation of the first two surface layers and fix the third and deeper layers in their ideal bulk positions to keep the computations tractable. This scheme

is consistent with the previous LEED analysis[6] where the two-layer relaxation model was used in the calculation of LEED I-V spectra. We determine the surface relaxation for each termination within two degrees of freedom, $d_{12}(\alpha)$ and $d_{23}(\alpha)$, which represent the fractional change of the first and the second interlayer spacings of the α termination. Because NiAl(111) shows a (1×1) LEED pattern,[6] reconstruction is not considered in the present calculations. We evaluate the total energies of 8 (7) different structures for a Ni (Al) termination to determine d_{12} and d_{23}.

For Ni/NiAl(111) we find that the total energy of the system is minimized at $d_{12}(\text{Ni})=-33\%$ and $d_{23}(\text{Ni})=0\%$ and the relaxation energy (25.5 mRy) per surface unit cell is very large [cf. 11.1 mRy in NiAl(110)]. Atomic position and valence-electron density at the unrelaxed and relaxed structures is shown in Fig. 2. The unrelaxed Ni/NiAl(111) [Fig. 2(a)] shows a significant charge redistribution around the second-layer Al sites. The mobile sp electrons spread into open space on the surface, especially into the hollow region on top of the third-layer Ni sites. The electron density around the fourth-layer Al sites is spherical and retains the bulk form. Each Ni atom on the first layer loses its four nearest-neighbor Al atoms and the lack of sp electrons in the surface region leaves the nearly filled d shell unscreened.

Our previous study[4] shows that the cohesion in NiAl can be characterized by the competition between the attraction due to interatomic d-electron bondings and the repulsion from compressed sp electron gas around the Al cores. In Ni/NiAl(111), a redistribution of the sp electrons around the second-layer Al sites allows the first layer to contract significantly into the bulk direction through an enhanced interatomic d bonding between the first and the third Ni layers [Fig. 2(b)]. The expansion of sp electron gas around the second-layer Al atoms is suppressed by the large contraction of the first-layer Ni atoms, and so the position of Al cores, which can be determined qualitatively by the electrostatic center of the electron charge distribution,[16] does not change much.

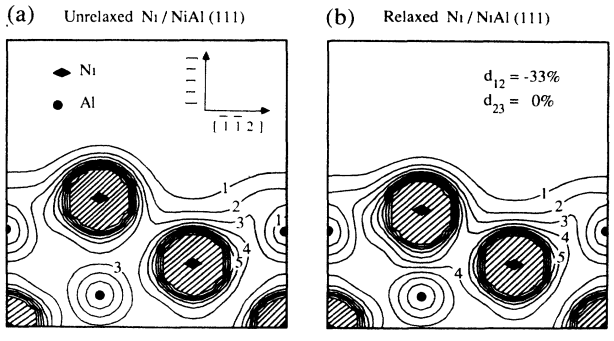

FIG. 2. Total valence-electron density of Ni/NiAl(111) before and after the relaxation. The electron density is represented by contours on a surface-normal plane parallel to $[\bar{1}\,\bar{1}\,2]$. The density unit is 0.01 e/a.u.^{3} and a uniform increment is used in the contour plots. The hatched regions represent a strongly localized d-electron density around the Ni cores.

The charge distribution around Al cores undergoes no notable changes through this relaxation, so the large relaxation energy of this surface seems to originate from the energy gain in the d bonding due to a large relaxation of the first Ni layer. The charge corrugation in the surface is somewhat reduced by this relaxation, but still the bare d electron lobes in the first layer protrude into the vacuum region and feel a highly repulsive potential. Thus, as will be discussed later, this structure shows many d electron surface and resonance features.

For Al/NiAl(111), we find that $d_{12}(\text{Al})=-16\%$ and $d_{23}(\text{Al})=-12\%$ and the relaxation energy (5.5 mRy) is very small compared to Ni/NiAl(111), which means that Al/NiAl(111) has a relatively stable electronic structure even in the ideal atomic geometry. This surface has plenty of delocalized sp electrons contributed from the first and the third Al layers, and the second-layer Ni atoms sit in a very stable bulklike NiAl environment. Therefore, in this termination, the redistribution of the surface sp electrons has a dominant role in determining the pattern of the atomic relaxation.

Al atoms in the first layer are surrounded by large open spaces (two threefold hollow sites) which are deeper in position than the first layer. Al/NiAl(111) is characterized by a large open space at the surface (threefold hollow sites). The high density of sp electrons around the first-layer Al sites fill this open space, and then the Al cores relax down to the bulk following the lowered electrostatic center of the electron gas. We note that the charge density around the first-layer Al sites shows a substantial change from the bulk form (Fig. 3), but little changes between before and after the relaxation. Because the interstitial sp electron distribution around the second-layer Ni atoms is similar to the bulk, the interlayer d-bonding enhancement is not as significant as in the case of Ni/NiAl(111), and most of the unstable surface and resonance features related to the first-layer Ni atoms in Ni/NiAl(111) disappear in the Al termination.

We summarize the present results and compare them with the LEED results[6] in Table I. The first row contains the fractional changes of the first two interlayer spacings (d_{12} and d_{23}) induced by the relaxation. To give a sense of the absolute motion of each atomic layer, these values

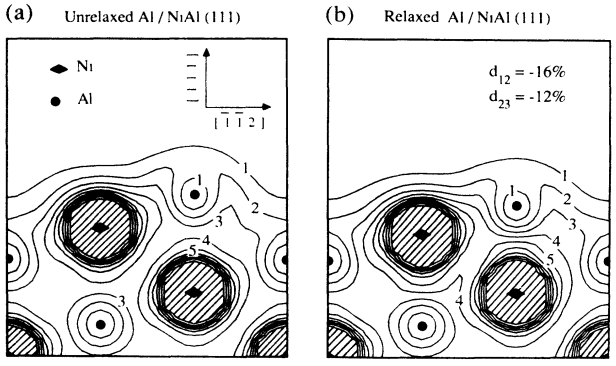

FIG. 3. Total valence-electron density of Al/NiAl(111) before and after the relaxation. The same convention as in Fig. 2 was used for this contour plot.

TABLE I. Relaxation patterns of the Ni- and Al-terminated NiAl(111) surfaces determined by the present theory and the previous LEED analysis (Ref. 6). The fractional change of the first two interlayer spacings (d_{12},d_{23}) are tabulated in the first row. In the second row d_1 and d_2 represent the fractional change in the position of the first and the second atomic layers relative to the ideal unrelaxed position. For comparison, we calculated the total energy of the LEED geometries and include the resulting relaxation energies per surface unit area in the last row.

	Ni/NiAl(111)		Al/NiAl(111)	
	Pseudopotential	LEED	Pseudopotential	LEED
d_{12}	−33%	−50%	−16%	−5%
d_{23}	0%	+15%	−12%	+5%
d_1	−33%	−35%	−28%	0%
d_2	0%	+15%	−12%	+5%
E_{relaxed}	−25.5 mRy	−22.0 mRy	−5.5 mRy	+3.5 mRy

are converted to the fractional changes (relative to d_0) of the position of the first two atomic layers (d_1 and d_2) in the next row. For a comparison of the energetics, we also calculated the total energy of the relaxed structures determined by the LEED analysis.

For Ni termination, there is good agreement between the present calculations and the previous LEED analysis. Both results show the same large contraction of the first Ni layer and a relatively small relaxation of the second Al layer. Though there exists a small difference in the magnitude of the second-layer relaxation, we find that both structures are very stable and energetically equivalent to each other with a large relaxation energy of similar magnitude.

For Al termination, however, there is a qualitative disagreement. Our calculation shows that both the first Al layer and the second Ni layer contract into the bulk direction. By contrast, in the relaxed geometry predicted by the LEED analysis, the first Al layer does not relax and the second Ni layer moves out into the vacuum region. Our prediction for the relaxation of Al/NiAl(111) is more acceptable from the following physical arguments. First, as seen from the fact that this surface is very open and the charge distribution around the first-layer Al cores undergoes a large change from the bulk configuration, one expects a large relaxation in that layer. More specifically, the *sp* electrons on top of the Al cores flow into the nearby threefold hollow regions, which strongly suggests an inward relaxation of the first-layer Al cores toward a lowered electrostatic center of the electron gas. Second, the openness of the surface requires that we should expect the second Ni layer and even the third Al layer to be affected by truncation of bulk NiAl. In that case, the redistribution of a high density of mobile *sp* electrons around the third-layer Al cores results in an inward relaxation of the second Ni layer since the interlayer (between the second and the fourth layer) *d*-electron bonding is enhanced through a reduction of the repulsive force maintained by the electron gas around the third Al layer. Therefore, an outward relaxation of the Ni layer is counterintuitive. Actually, it turns out from our total-energy calculations that this LEED structure is very unstable energetically: its total energy is higher than that of the unrelaxed Al/NiAl(111).

III. ELECTRONIC STRUCTURE OF NiAl(111)

In this section we study the surface electronic band structure of NiAl(111), which is sensitive to the underlying atomic structure. We investigate which termination occurs on the NiAl(111) surface by comparing angle-resolved ultraviolet photoemission spectroscopy (ARUPS) measurements with the pseudopotential band structure of a Ni- and an Al-terminated NiAl(111) surface.

A. Surface states measured by ARUPS

The angle-resolved-photoemission experiment on NiAl(111) was carried out at the National Synchrotron Light Source at Brookhaven National Laboratory (Upton, NY). Radiation from the 750-MeV vacuum-ultraviolet storage ring was dispersed by a dual toroidal grating monochromator yielding photons in the $10<\hbar\omega<120$ eV range.[17] Photoelectrons were energy analyzed with a hemispherical electrostatic analyzer with an acceptance angle of ±2°. The combined instrumental resolution (photon and electron) is about 0.13 eV for $\hbar\omega<35$ eV and increases linearly with photon energy to 0.30 eV for $\hbar\omega=60$ eV. Details of the angle-resolved analyzer and the vacuum chamber were described elsewhere.[18]

The (111) crystal face of NiAl was cleaned by cycles of neon-ion bombardment followed by annealing to 850 °C for 10 min to restore a well-ordered (1×1) surface as indicated by LEED. The average surface composition of the sample was studied by x-ray photoelectron spectroscopy (XPS) takeoff-angle measurement prior to the photoemission experiment. The XPS analysis showed that the NiAl(111) sample has an average surface composition that is similar to the bulk composition of 50.6±2.0 at. % Al. This composition was determined by Paschen optical-emission spectroscopy and the use of standard solutions. In addition, spark source mass spectroscopy was invoked to insure that there were no major impurities in the sample (total < 100 wt. ppm). Once the crystal is clean, the surface is free of contaminants for 30 min at an operating pressure of 2×10^{-10} Torr. During the course of the experiment, the sample is repeatedly cleaned in every 30 min to be contamination-free. The cleanness of the surface is monitored by the appearance of the oxygen 2*p* peak which has a binding energy of 6 eV in the valence-band region.

The (111) crystal face of a CsCl structure is shown in Fig. 1(a) and the corresponding two-dimensional unit cell is indicated by a parallelogram. Notice the first three layers of atoms are exposed. Along the ⟨112⟩ direction, the atomic arrangements of the first three layers in the positive and negative directions are not equivalent [Fig. 1(b)].

Thus, as the bulk Brillouin zone is projected onto the surface Brillouin zone (SBZ), the two $\bar{M}$ points in the SBZ are not equivalent and the symmetry is reduced to threefold symmetry. This is illustrated in Fig. 1(c). Our convention is to distinguish these two inequivalent points as $\bar{M}_+$ and $\bar{M}_-$, as determined from our bulk band measurements. $\bar{\Gamma}\bar{M}_+$ is along the $[\bar{2}11]$, $[11\bar{2}]$, and $[1\bar{2}1]$ directions, while $\bar{\Gamma}\bar{M}_-$ is along the $[2\bar{1}\,\bar{1}]$, $[\bar{1}\,\bar{1}2]$, and $[\bar{1}2\bar{1}]$ directions. Along the $\langle 110\rangle$ direction, however, the atomic arrangements in the positive and negative directions are the same. Thus, all the $\bar{K}$ points in the SBZ are equivalent. Since the crystal mirror plane is along the $\langle 112\rangle$ direction in real space ($\bar{\Gamma}\bar{M}$ in reciprocal space), we will discuss the reflection symmetry of the initial state wave function with respect to this mirror plane.

1. *Surface states at $\bar{\Gamma}$: Normal emission*

For normal emission, the analyzer collects photoelectrons emitted from the $\bar{\Gamma}$ point of the (111) SBZ. This measurement is made to determine the symmetry and the energy of the initial states which are dipole allowed for normal emission. Along the [111] direction of the cubic Brillouin zone, dipole selection rule limits the allowed transition to the Λ_1 and Λ_3 initial states. The Λ_2 initial state is dipole forbidden (top half of Table II). The top half of Table II gives the symmetries of the initial-state wave functions for normal emission polarization measurements. By utilizing the polarized radiation from the storage ring, initial states with Λ_1 symmetry would be observed when the electric field of the incident light, **A**, is normal to the surface, and states with Λ_3 symmetry would be observed when **A** lies in the plane of the surface (*s* polarization).

Figure 4 shows the symmetry of the Λ_1 and Λ_3 bands at $\hbar\omega=20$ eV. The schematics on the right show the **A** vector with respect to the (111) surface in real space. The Λ_1 band is A_z (along the [111] direction) excited while the Λ_3 band is A_x (along the $[\bar{1}\bar{1}2]$ direction) excited. In Fig. 4, bulk peaks with Λ_1 and Λ_3 symmetry are indicated by arrows. The hatched peaks are surface states which do not disperse with photon energy. Since the surface states exhibit well-defined symmetry as the bulk states, i.e., they both have a strong polarization dependence, we will use bulk band symmetry notation for the two surface states. The Λ_1 surface state displayed in the upper panel is excited by A_z and has a binding energy of 2.85 ± 0.10 eV while the Λ_3 surface state displayed in the lower panel is excited by A_x and has a binding energy of 0.80 ± 0.10 eV.

TABLE II. Symmetry of initial states along ΓR.

	Normal emission	
A	Dipole allowed	Dipole forbidden
A_x ($x=[\bar{1}\bar{1}2]$)	Λ_3	Λ_2
A_z ($z=[111]$)	Λ_1	Λ_2
	Off-normal emission	
$A_\parallel$	Even states	Odd states
$\bar{\Gamma}\bar{M}$	Λ_1	Λ_3

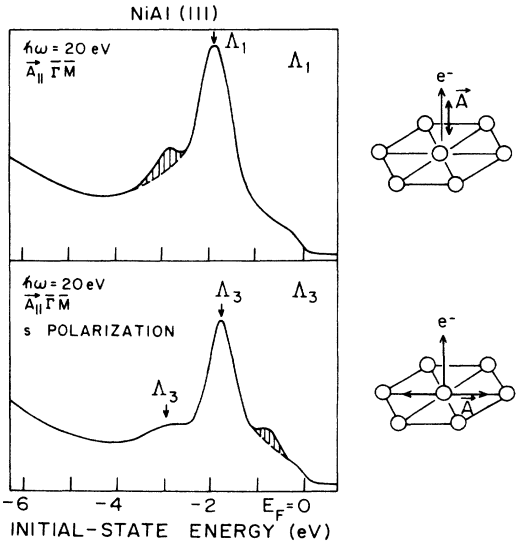

FIG. 4. Normal-emission photoemission spectra showing (a) the Λ_1 initial states and (b) the Λ_3 initial states. Bulk states are indicated by arrows. Hatched peaks are surface states.

Figure 5 shows a set of typical photoemission spectra for several photon energies of these surface states. Both the Λ_1 and Λ_3 surface states (hatched peaks) are well separated from the bulk bands. However, they do not exhibit appreciable intensity over the range of photon energy displayed in Fig. 5 with the exception for the Λ_1 surface state at $\hbar\omega=14$ eV. A more pronounced intensity variation of the Λ_3 surface state with photon energy is found at point $\bar{M}$ and is discussed in the following.

2. *Surface states at $\bar{M}$: Off-normal emission*

For NiAl(111), the only crystal mirror planes are along the $\langle 112\rangle$ directions in real space or along the $\bar{\Gamma}\bar{M}$ direction of the SBZ in reciprocal space. This can be seen from the surface geometry given in Fig. 1(a). From our normal emission measurement (at point $\bar{\Gamma}$ of the SBZ), the surface state observed at -0.80 eV has a Λ_3 symmetry while the surface state observed at -2.85 eV has a Λ_1 symmetry. Away from point $\bar{\Gamma}$, the wave-function symmetry of the surface states are reduced and can be discussed as either even or odd with respect to the reflection about the crystal mirror plane. For convenience, we will continue to use the same symmetry notations for the two surface states given at point $\bar{\Gamma}$ for measurements made away from the zone center.

Along $\bar{\Gamma}\bar{M}$, the Λ_3 surface state has odd reflection symmetry while the Λ_1 surface state has even reflection symmetry. This is given in the lower half of Table II. As the analyzer is moved away from the surface normal, the photoelectron collected has a finite momentum, $\mathbf{k}_\parallel$, parallel to the surface as given by the following expression,

$$k_\parallel = 0.512\sqrt{\hbar\omega - E_b - \phi}\,\sin\theta_e \ \text{Å}^{-1}\,, \tag{1}$$

where E_0 is the electron binding energy, θ_e is the emission angle with respect to the surface normal, and ϕ is the

crystal work function. Following Eq. (1), we can change photon energy and the emission angle in such a way that $\mathbf{k}_{\parallel}$ is always kept at point $\overline{M}$ ($k_{\parallel}=0.89$ Å^{-1}). The purpose of doing this measurement is to obtain both the binding energies and the photoelectric cross sections for the two surface states at point $\overline{M}$. Since the measurement is made away from the surface normal, we need to first show that the Λ_3 (Λ_1) surface state has odd (even) symmetry away from point $\overline{\Gamma}$.

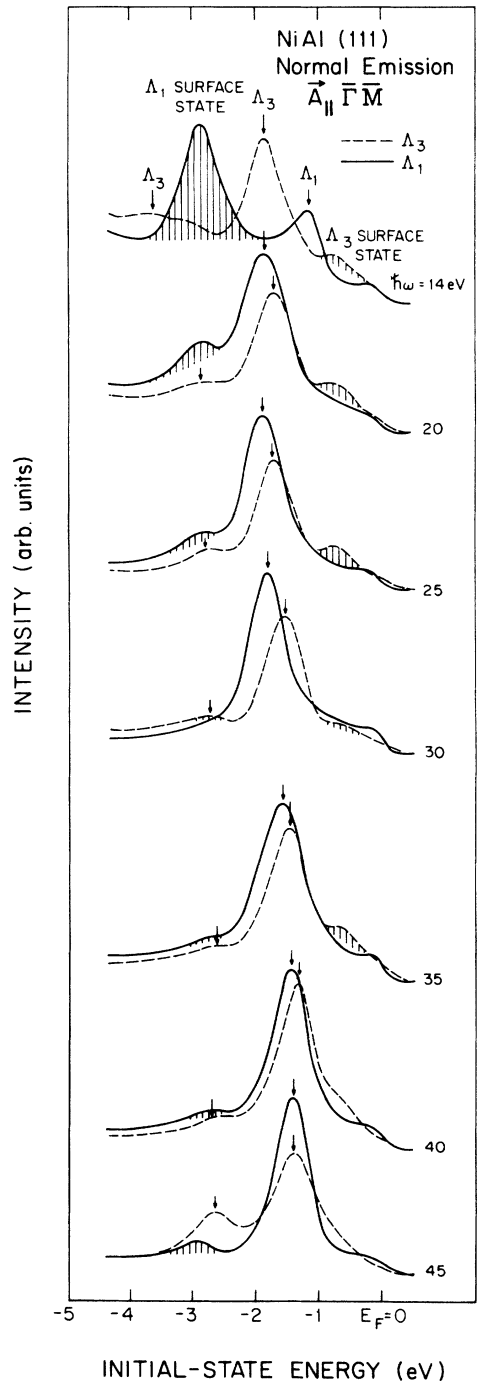

FIG. 5. Energy-distribution curves showing the Λ_1 and Λ_3 surface states (hatched peaks) and the bulk transitions (indicated by arrows).

Figure 6 shows photoemission spectra taken at $\hbar\omega=20$ eV for $\mathbf{k}_{\parallel}$ at points $\overline{M}_+$ and $\overline{M}_-$. Two energy-distribution curves (EDC's) are shown for points $\overline{M}_+$ and $\overline{M}_-$, respectively. Solid (dashed) curves represents the spectra with even (odd) reflection symmetry with respect to the ⟨112⟩ mirror plane. From this figure, it is obvious that the Λ_3 surface state has odd symmetry away from point $\overline{\Gamma}$.

Figure 7 shows a sequence of photoemission spectra taken at points $\overline{M}_+$ and $\overline{M}_-$ as a function of photon energy. These spectra were taken at odd collection geometry. In this figure, bulk transitions are indicated by "*A*" and "*B*." The stationary peak at −0.80 eV (connected by the dashed lines) appeared in both points $\overline{M}_+$ and $\overline{M}_-$ can be identified as the Λ_3 surface state. Since the binding energy of this surface state is the same at points $\overline{\Gamma}$ and $\overline{M}$, it must be a very localized *d* state originated from the Ni site.

The intensity variation of the Λ_3 surface states at points $\overline{M}_+$ and $\overline{M}_-$ is shown in Fig. 8. The data points shown in this figure are normalized by using the signal from a calibrated tungsten mesh such that variation in the photon flux with photon energy has been removed. The intensity of the Λ_3 surface state is approximately five times stronger at point $\overline{M}_-$ than at point $\overline{M}_+$. This intensity difference is due to the difference in final-state

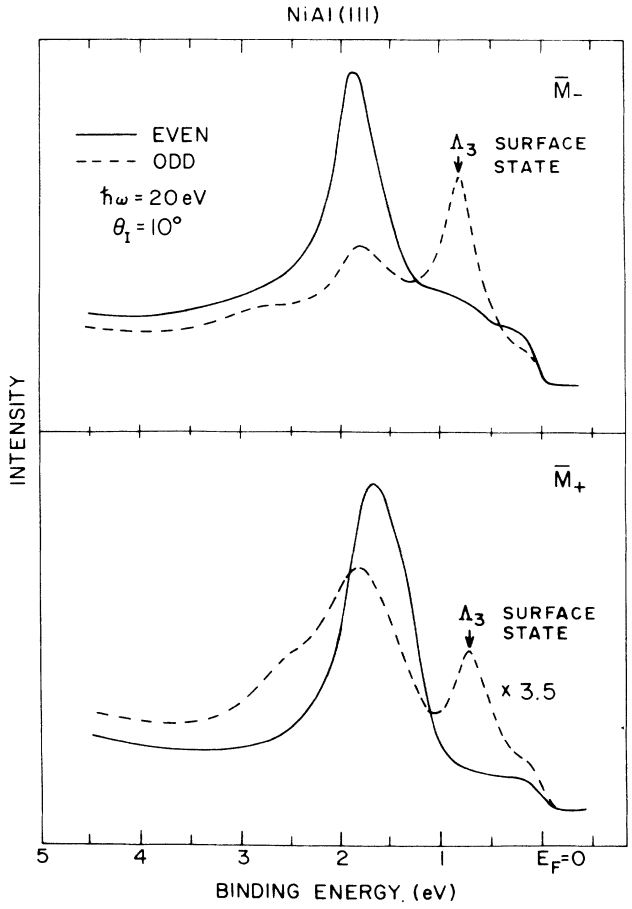

FIG. 6. Photoemission spectra taken at points $\overline{M}_+$ and $\overline{M}_-$. The Λ_3 surface state is shown to have odd symmetry.

scattering of the surface state measured at points $\bar{M}_+$ and $\bar{M}_-$. Besides the intensity difference, the Λ_3 surface state is found to peak at slightly different photon energies for the two $\bar{M}$ points. The curve for point $\bar{M}_-$ shows a single maximum around 40 eV photon energy while two additional maxima are shown for point $\bar{M}_+$ at 26 and 100 eV. Since the two $\bar{M}$ points are not equivalent at the surface, the intensity variation with photon energy of the surface state measured at each $\bar{M}$ point is expected to be different.

For the Λ_1 surface state with even reflection symmetry, an examination of the calculated bulk projection of even symmetry states along $\bar{\Gamma}\bar{M}$ shows a band gap at point $\bar{\Gamma}$ between -2.2 and -3.0 eV [Fig. 11(a)]. This bulk gap extends from point $\bar{\Gamma}$ to about the middle of the SBZ along the $\bar{\Gamma}\bar{M}$ direction. Since there is no band gap at point $\bar{M}$, we do not expect the Λ_1 surface state to be observed at $\bar{M}$. It will be shown in the following section that the dispersion of this surface state was observed only in the bulk band gap which exist over half of the surface zone.

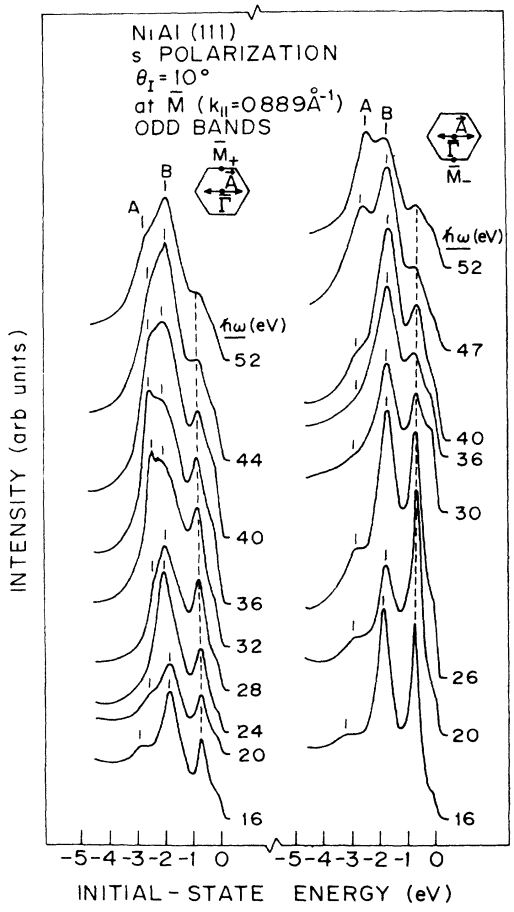

FIG. 7. Photoemission spectra taken at points $\bar{M}_+$ and $\bar{M}_-$. The Λ_3 surface state at each photon energy is joined by the two vertical dashed lines. Peaks denoted by "*A*" and "*B*" are bulk states.

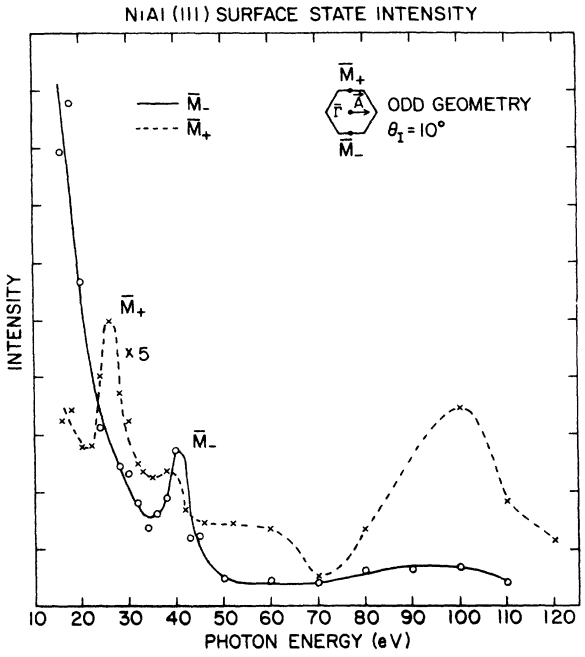

FIG. 8. Intensity variation of the Λ_3 surface state as a function of photon energy at points $\bar{M}_+$ and $\bar{M}_-$.

3. *Dispersion of surface-state bands*

The dispersion of the two surface-state bands was measured along the $\bar{\Gamma}\bar{M}$ direction in the SBZ. Measurements of the odd Λ_3 surface band dispersion were done at several $\mathbf{k}_{\parallel}$ points from point $\bar{\Gamma}$ to point $\bar{M}$. Figure 9

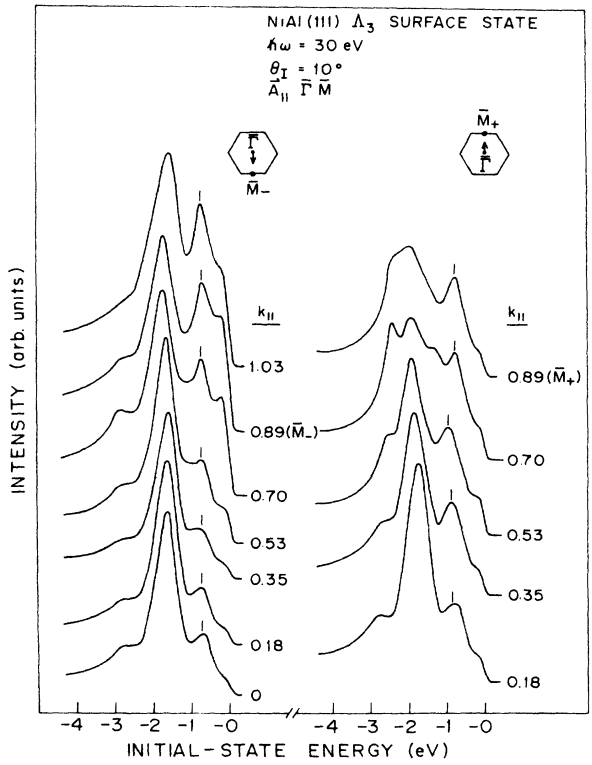

FIG. 9. Dispersion of the Λ_3 surface state along $\bar{\Gamma}\bar{M}$. The lack of dispersion of this surface state indicates that it is a localized Ni *d* state. The unit of $k_{\parallel}$ is Å^{-1}.

shows the dispersion of the Λ_3 surface band along lines $\bar{\Gamma}-\bar{M}_+$ and $\bar{\Gamma}-\bar{M}_-$. The apparent lack of dispersion of this surface-state band indicates that its wave function is very localized and is likely from a Ni d state.

For the even Λ_1 surface band, the dispersion was measured along $\bar{\Gamma}\bar{M}$. Figure 10 shows that this surface band (indicated by vertical bars) moves to a lower binding energy away from point $\bar{\Gamma}$ and disappears half way across the surface zone where it probably runs into the very intense bulk peak at -1.80 eV. A discussion of the measured and calculated surface-state bands will be given in the following section.

B. Calculated surface-state band structure

In this section we give a theoretical description of the electronic structure of both Ni/NiAl(111) and Al/NiAl(111) the atomic structures of which have been determined in Sec. II. We calculate the band structures of both the relaxed Ni/NiAl(111) and the relaxed Al/NiAl(111) on a high-symmetry line, $\bar{\Gamma}\bar{M}$, and determine the character of each surface-state band. Note that point $\bar{M}_+$ is equivalent to point $\bar{M}_-$ in the slab geometry through an inversion symmetry. The variations in the electronic feature between both terminations are closely examined and are compared to the measured band structure, which yields information on the termination of NiAl(111).

We begin with Ni/NiAl(111). Figure 11 shows the calculated surface- and resonance-state bands along $\bar{\Gamma}\bar{M}$. The band structure is divided into two symmetry subspaces according to the reflection symmetry about a surface-normal mirror plane. The projected bulk band structure of NiAl is included as a shaded region to clearly isolate surface states. A solid (dashed) band represents a surface- (resonance-) state band. Our convention is to distinguish a surface- (resonance-) state from bulk states as one that contains more than 70% (50%) of the charge in the first two atomic layers and whose eigenvalue is either in a symmetry gap or very close to an edge of a gap.

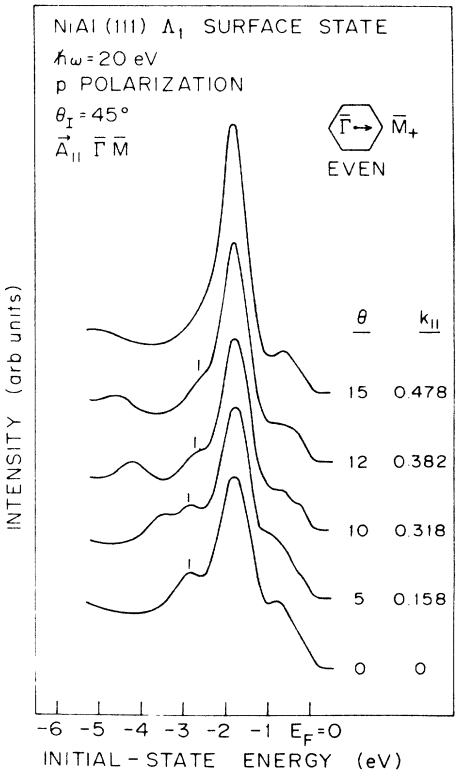

FIG. 10. Dispersion of the Λ_1 surface state along $\bar{\Gamma}\bar{M}$. The unit of $k_{\parallel}$ is Å^{-1}.

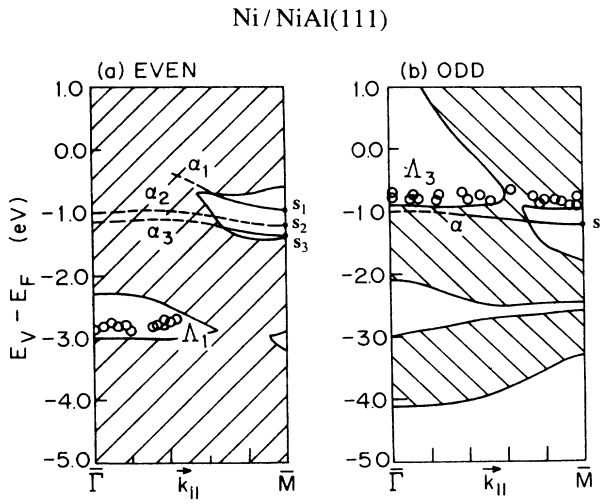

FIG. 11. Calculated surface and resonance band structure of the relaxed Ni/NiAl(111) along $\bar{\Gamma}\bar{M}$: (a) represents even-symmetry states, (b) represents odd-symmetry states, solid (dashed) lines represent surface (resonance) states, and the hatched regions are the projected bulk band structure. Open circles represent the ARUPS measurements.

We note in Fig. 11 that most of surface and resonance states are localized within 1.5 eV below the Fermi energy and form nearly dispersionless bands of d character. In fact, we find that the charge-density distribution of the surface states has a strong d character localized on the surface Ni cores. The charge character of a representative surface state (denoted by s, s_1, s_2, and s_3 in Fig. 11) in each band is shown in Fig. 12, where we note that sp character is negligible in these surface states except for s_2 state. These states originate from the bulk states at band-gap edges. Unscreened d electron lobes in the first layer feel a strong repulsive potential introduced by an elimination of the other half of the bulk. As a result, some electrons in the bulk level are pushed into a gap as resonance modes. This behavior is reflected well in the total electron density-of-states (DOS) curves shown in Fig. 13(a). We note a significant change in the DOS curve between bulk NiAl and Ni/NiAl(111). A large portion of the bulk d states (bound at ~ -2.0 eV) are shifted to the higher-energy states (at ~ -1.2 eV) in Ni/NiAl(111). Although this severe change includes some artifact originating from a finite-slab calculation, it represents well at least the main character of the Ni-terminated NiAl(111).

As we see in Fig. 13(b), the overall DOS curve for Al/NiAl(111) has a very similar shape to that of bulk NiAl. The main effect of an additional Al layer on the surface electronic structure is to quench most of the d

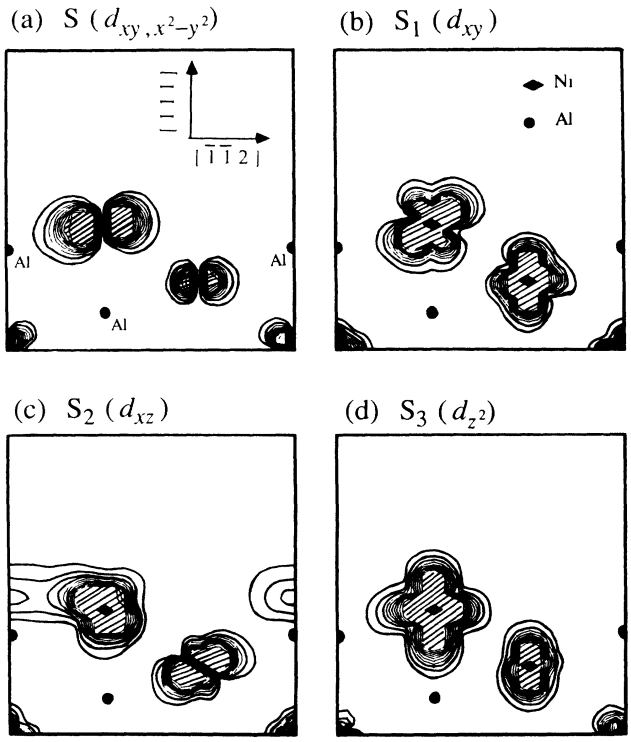

FIG. 12. Charge characters of the representative surface states shown in Fig. 11: surface state (a) s (d_{xy,x^2-y^2}), (b) s_1 (d_{xy}), (c) s_2 (d_{xz}), and (d) s_3 (d_{z^2}). A uniform increment (0.5×10^{-3} e/a.u.^{3}) is used in the contour plot.

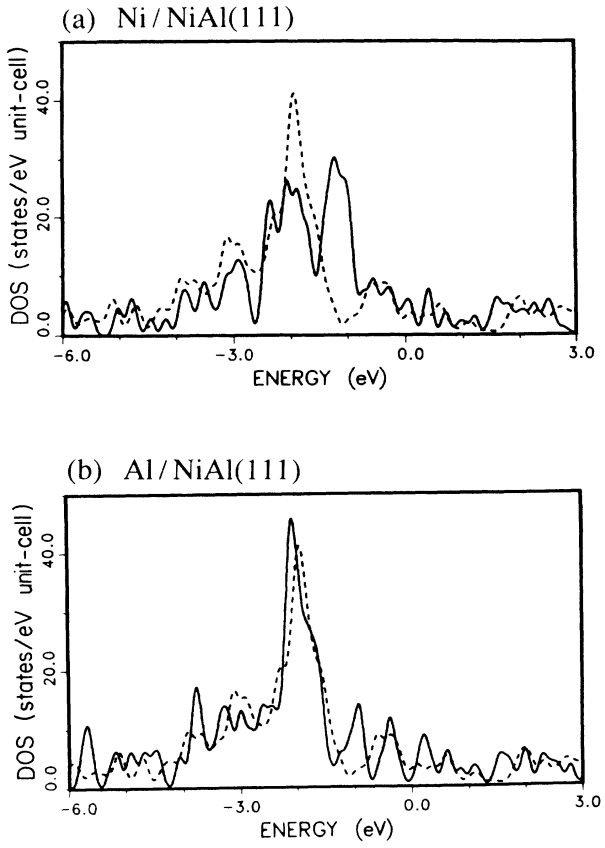

FIG. 13. Calculated electron density of states (DOS) as a function of binding energy for the relaxed Ni/NiAl(111) and Al/NiAl(111). Solid lines represent the DOS of a slab unit cell and dashed lines represent the DOS of bulk NiAl that is included as a reference.

resonance states. Owing to the surface Al layer, the otherwise bare Ni atoms in the next layer are placed in a high density of *sp*-electron gas and recover a fairly stable configuration close to that found in the bulk. In Al/NiAl(111), therefore, most of *d* resonance states present in Ni/NiAl(111) are pulled down nearly to their original bulk values. As a result, we find that many *d* resonance bands disappear in the band structure of Al/NiAl(111) in Fig. 14. While losing the strong surface features of *d* character at -1.0 eV, this Al termination creates a new surface electronic feature not present in Ni/NiAl(111), which is found at -2.7 eV in the middle of an even-symmetry gap and is strongly related to the surface Al layer with a mixed character of *d* and *sp* electron. The charge character of a representative surface state (s, s_1, and s_2 in Fig. 14) of each band is shown in Fig. 15. Even at Al/NiAl(111), *d* character is still strong in the surface states, but we note that these surface states are somewhat affected by the first-layer Al atoms, i.e., a moderate mixing of *sp* character is observed in each surface state. This *sp* character is especially significant for the state s at -2.7 eV [Fig. 15(a)].

Now we compare the above calculated band structures with the ARUPS measurements presented in the previous section. We have measured the dispersions of two surface features along the $\bar{\Gamma}\bar{M}$ symmetry line; one strong surface-state band (Λ_3) at -0.8 eV in the odd-symmetry subspace and the other weaker resonance band (Λ_1) at -2.8 eV in the even space. These two measured bands are represented by open circles in Figs. 11 and 14. The

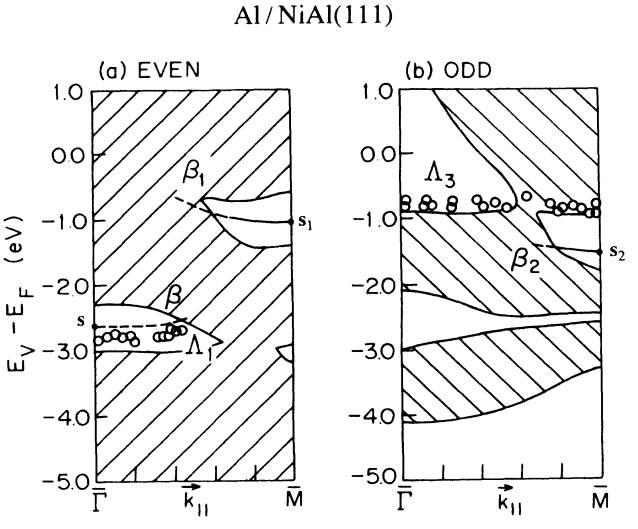

FIG. 14. Calculated surface and resonance band structure of the relaxed Al/NiAl(111) along $\bar{\Gamma}\bar{M}$: (a) represents even-symmetry states, (b) represents odd-symmetry states, solid (dashed) lines represent surface (resonance) states, and the shaded region is the projected bulk band structure. Open circles represent the ARUPS measurements.

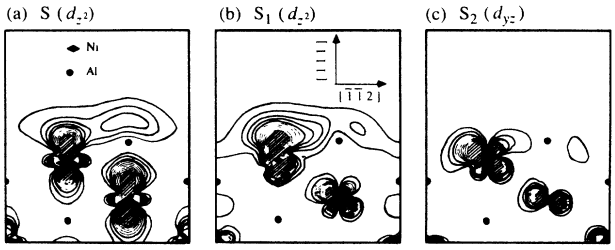

FIG. 15. Charge characters of the representative surface states shown in Fig. 14: Surface state (a) s (d_{z^2}), (b) s_1 (d_{z^2}), and (c) s_2 (d_{yz}). A uniform increment (0.5×10^{-3} e/a.u.^{3}) is used in the contour plot.

Λ_3 surface-state band extends to the whole SBZ with a negligible dispersion. The Λ_1 surface-state band disperses slightly up towards the Fermi level from point $\bar{\Gamma}$ to point $\bar{M}$ and loses its surface feature in the middle of the SBZ.

By comparing the binding energy and the dispersion of the measured bands with those of the calculated surface and resonance bands, we find that the calculated band α in Ni/NiAl(111) looks close to the measured band Λ_3, and the calculated band β in Al/NiAl(111) to the other measured band Λ_1. The agreement in the binding energy is quite good within a generally acceptable discrepancy ($\sim\pm0.3$ eV) between the calculations and the ARUPS measurements. This comparison shows that the measured surface band structure has a common feature partly with a Ni termination and partly with an Al termination, suggesting that the real NiAl(111) surface is possibly composed of both Ni- and Al-terminated (111) domains. In conclusion, the present study of the electronic structure of NiAl(111) supports a structural model suggested by the previous LEED analysis. At this point, however, it is worthwhile to point out that the comparison of only two measured bands with calculations is not sufficient to lead to a solid conclusion. In addition, it is not clear why the calculated strong resonance bands, which appear in both terminations at around -1.0 eV in the even-symmetry space, are not detected in the ARUPS experiment.

IV. SUMMARY

We applied the pseudopotential total-energy-calculation scheme to the study of NiAl(111). The relaxation patterns of the two outermost atomic layers were determined for two possible terminations by minimizing the total energy of the systems. For a Ni-terminated NiAl(111) surface we obtained that $d_{12}(\mathrm{Ni})=-33\%$ and $d_{23}(\mathrm{Ni})=0\%$ and, for an Al termination, $d_{12}(\mathrm{Al})=-16\%$ and $d_{23}(\mathrm{Al})=-12\%$. We found that the results obtained by a LEED analysis are in good agreement with our results for a Ni termination, but predict a qualitatively different structure for an Al termination, which turned out to be very unstable energetically, i.e., it has a total energy higher than that of the unrelaxed surface.

We also compared the experimental surface band structure with those calculated at the relaxed geometry for each termination. We found that the measured surface band structure has a common feature not only to that of Ni/NiAl(111), but also to that of Al/NiAl(111). This feature of the electronic structure supports that two different domains, Ni/NiAl(111) and Al/NiAl(111), coexist in a real NiAl(111) surface.

ACKNOWLEDGMENTS

This work was supported at the University of Pennsylvania by the National Science Foundation through the Materials Research Laboratories Program under Grant No. DMR-85-19059 and at Oak Ridge National Laboratory by the U.S. Department of Energy under Contract No. DE-AC05-84OR21400. Calculations were carried out using the Cray Research, Inc. X-MP/48 supercomputer at the Pittsburgh Supercomputing Center.

*Present address: Department of Physics, The Ohio State University, 174 West 18th Avenue, Columbus, Ohio 43210-1106.
†Present address: P.O. Box 709, Brookhaven National Laboratory, Upton, New York 11973.

[1]H. L. Davis and J. R. Noonan, Phys. Rev. Lett. **54**, 566 (1985).
[2]S. M. Yalisove and W. R. Graham, Surf. Sci. **183**, 556 (1987).
[3]S. P. Chen, A. F. Voter, and D. J. Srolovitz, Phys. Rev. Lett. **57**, 1308 (1986).
[4]M. H. Kang and E. J. Mele, Phys. Rev. B **36**, 7371 (1987).
[5]J. I. Lee, C. L. Fu, and A. J. Freeman, Phys. Rev. B **36**, 9318 (1987).
[6]J. R. Noonan and H. L. Davis, Phys. Rev. Lett. **59**, 1714 (1987).
[7]A recent analysis of the low-energy ion-scattering data also leads to the same conclusion: H. Niehus, Nucl. Instrum. Methods B **33**, 876 (1988).
[8]R. Franchy, M. Wuttig, and H. Ibach, Surf. Sci. **189/190**, 438 (1987).
[9]J. Wendelken (unpublished).
[10]P. Hohenberg and W. Kohn, Phys. Rev. **136**, B864 (1964).
[11]W. Kohn and L. J. Sham, Phys. Rev. **140**, A1133 (1965).
[12]D. M. Ceperley and B. J. Alder, Phys. Rev. Lett. **45**, 566 (1980).
[13]J. P. Perdew and A. Zunger, Phys. Rev. B **23**, 5048 (1981).
[14]M. H. Kang, R. C. Tatar, E. J. Mele, and P. Soven, Phys. Rev. B **35**, 5457 (1987).
[15]I. Morrison, M. H. Kang, and E. J. Mele, Phys. Rev. B **39**, 1575 (1989).
[16]M. W. Finnis and V. Heine, J. Phys. F **4**, L37 (1974).
[17]B. P. Tonner, Nucl. Instrum. Methods **172**, 133 (1980).
[18]C. L. Allyn, T. Gustafsson, and E. W. Plummer, Rev. Sci. Instrum. **49**, 1197 (1978).